Journal of Inorganic and Organometallic Polymers and Materials (2023) 33:1298–1305
https://doi.org/10.1007/s10904-023-02570-7

RESEARCH

A Photochromic Thienyl Containing Zinc-Organic Framework with Three-Fold Interpenetrating Arrangement Showing Reversible Switching Photoconducting Property

Aidong Tan[1,2] · Jie Zhang[1] · Jinhua Piao[3] · Jiayao Li[1] · Zhiyong Fu[1]

Received: 2 July 2022 / Accepted: 31 January 2023 / Published online: 1 March 2023

Abstract

Exploring novel photoconductance switch crystalline materials with color indication is of the utmost importance. Herein, we reported a photochromic and photoconductive zinc organic framework, $[Zn_2(TDC)_2(TPT)]\cdot H_2O$, composed of electron-rich sulfur-containing compounds, 2,5-thiophenedicarboxylic acid (TDC), as electron donor, and electron-deficient 2,4,6-tri-(4-pyridyl)-*s*-triazine (TPT) as the electron acceptor, which exhibited an uncommon electron transfer pathway. Upon photo-stimuli and subsequently storing in dark, the crystalline materials show reversible color changes from pale-yellow to green accompanied by the conductance switching from 4.3×10^{-9} to 1.9×10^{-9} S cm^{-1}. The mechanism and electron transfer pathway of the stimuli-responsive materials have been explained by X-ray photoelectron spectroscopy (XPS), electron spin-resonance spectroscopy (ESR), and single X-ray diffraction data. Upon light exposure, the electron could hop from both thienyl-S/carboxyl-O to *s*-triazine-N. This work not only offers a new approach to the modification of visible photoconducting switch by the crystal engineering strategy but also sheds light on a new electron transfer system.

Graphical Abstract

A single crystalline photoconductance switch with color indication has been constructed based on the thienyl-containing photosensitive zinc organic framework. It shows reversible color changes from yellow to green accompanied by conductance switching from 4.3×10^{-9} to 1.9×10^{-9} S·cm^{-1}.

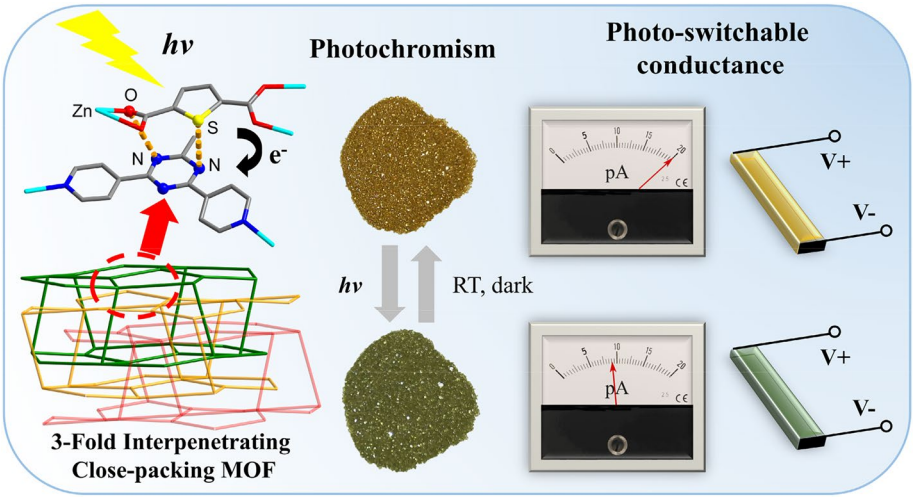

Keywords Thienyl containing zinc-organic framework · Photo-responsive system · Crystalline material · Structure and property

Extended author information available on the last page of the article

1 Introduction

Developing molecule-based materials with tuneable electrical conductivity properties is of great interest for their potential wide applications in energy storage and electronic devices, such as photovoltaic, thermoelectric batteries, and supercapacitors [1–3]. Particularly, semiconductors with the reversible altering of both electrical conductivity and color upon external stimuli can serve as smart switches and detectors in many devices both visual and electronic responses [4, 5]. Among various molecular systems, metal–organic frameworks (MOFs) bring convenience for integrating photosensitive and conducting characters into single crystalline devices for their well-defined structures that can be tailored by selecting metal ions and ligands [6–8]. Recently, various interesting photochromic systems are built via the assembly of electron donors (D) and acceptors (A) units with metal–ligand connections [9–11]. It is established that light-driven electron transfer can proceed in the well-ordered D–A assembling framework, and simultaneously alter the physical properties of the materials, such as photochromism, magnetism, and conductance [12–14]. Many stimuli-responsive D–A systems have been explored by combining electron-deficient N-containing heterocyclic components as electron acceptor and electron-rich halogen or oxygen from carboxyl group units as electron donor [15–17]. Benefitting from better chemical stability, structural tunability, and fatigue resistance of MOFs frameworks, the electron transfer path could be established by the appropriate selection of D and A building blocks and the control structure [18, 19]. For the acceptor, 2,4,6-tri-(4-pyridyl)-*s*-triazine (TPT) molecule is well-used for its electron-deficient character and planar rigid structure facilitating electron capture. In addition, it features a 3-connected linker that helps to construct 2D or 3D coordination networks [20–22]. Nevertheless, for the donor selection of existing D–A systems, few reports go beyond halogen or oxygen donors [7, 23]. Electron-rich sulfur-containing compounds, such as fulvalene, thiophene mercaptan and inorganic nanomaterials, have been well used to build conductive charge-transfer complexes as charge donors for rapid electron transport [24–29]. Given novel photoconductance switch materials constructed via integrating photosensitive and conducting characters into single crystalline devices, S-containing ligand 2,5-thiophenedicarboxylic acid (TDC) and TPT molecules are used to build new D–A based photoelectric sensitive systems.

Herein, a MOF based photoconductance switch $[Zn_2(TDC)_2(TPT)]\cdot H_2O$ (**1**) is prepared via the zinc-ligands coordination assemblies with 2,5-thiophenedicarboxylic acid (TDC) and 2,4,6-tri-(4-pyridyl)-*s*-triazine (TPT) as the electron donors and acceptors respectively. In the three-fold interpenetrating close-packing structure, TDC and the N-heterocyclic moiety (triazine) of TPT stack in an offset mode, satisfying the requirement of electron transfer between the D–A units. Its reversible photochromic behaviors featuring from pale-yellow to green upon light stimuli are coupled with the photoconductance characters showing conductivity from 4.3×10^{-9} to 1.9×10^{-9} S cm^{-1}. As evidenced by X-ray photoelectron spectroscopy (XPS) and electron spin-resonance spectroscopy (ESR) data, it is interesting to observe that the photo-induced electrons not only hop from traditional carboxylate groups in TDC to electron-deficient TPT, but also transfers from electron-rich thienyl-S to acceptor TPT, which decreases the conductivity of **1**. And this builds a fascinating single crystalline photoconductance switch with color indication.

2 Experimental Section

2.1 Synthesis of $[Zn_2(TDC)_2(TPT)]\cdot H_2O$ (1)

$[Zn_2(TDC)_2(TPT)]\cdot H_2O$ (**1**) was solvent-thermally synthesized utilizing a 25.0 mL Parr Teflon lined stainless steel reactor. $Zn(NO_3)_2\cdot 6H_2O$ (150.0 mg, 0.50 mmol), 2,5-thiophenedicarboxylic acid (TDC, 51.60 mg, 0.30 mmol), TPT (62.0 mg, 0.20 mmol), H_2O (4.0 mL) and 2-Ethoxyethanol (6.0 mL) was allowed to go through a static reaction at 125 °C for 48 h before it was gradually cooled to room temperature in 1000 min. Pale yellow prism crystals, **1**, were separated by filtration and washed with DI water and EtOH several times to give about 59.30% yield (95.0 mg, based on TPT). Anal. Calcd. (found, %) for $C_{30}H_{18}N_6O_9S_2Zn_2$ (*fw.* 801.36), C: 44.96 (45.18); N: 10.48 (10.25); S: 8.00 (7.93); H: 2.26 (1.37).

2.2 Structure Determinations

Single crystals of **1** before and after light-irradiation (the samples were irradiated by Xe lamp for 20 min to ensure sufficient discoloration) were selected under an optical microscope and data collection was performed on an Agilent SuperNova diffractometer with a graphite monochromatic Mo/$K\alpha$ radiation ($\lambda=0.71073$ Å) at 150 K. Empirical absorption correction was applied for the data sets that was made with the MUTI-SCAN program for **1**. The structure was solved by direct methods using SHELXS-2014 and refined on F^2 by full-matrix least-squares techniques using SHELXL-2014. All non-hydrogen atoms were located from iterative examination of difference *F*-maps following least squares refinements of the earlier models and treated anisotropically. The positions of hydrogen atoms were generated geometrically. The solvent water molecule is disordered over

three positions with 0.5, 0.3 and 0.2 respectively. The structure was examined using the Addsym subroutine PLATON to assure that no additional symmetry could be applied to the models. More details on crystallographic information have been deposited in the *cif* format as CCDC-2035073 (before) and 2054909 (after) in the Cambridge Crystallographic Data Centre.

2.3 Optical Absorption Spectrum and Conductivity Measurement

UV–Vis spectral measurements were carried out using a HITACHI U-3010 spectrometer, and a $BaSO_4$ plate was used as a 100% reflectance standard. A Xenon lamp (CEL-TCX250, 250 W, 290–800 nm, light intensity 400 mW cm^{-2}) was used as the light-irradiation source, and UV–vis spectral changes of the compound were collected after the powder samples irradiated at different times (viz. 30 s, 1 min, 2 min, 4 min and 6 min) by Xe lamp.

A homemade device was used to test the electrical conductivities of the single crystal. Two 125 μm Ag wires were pasted on both sides of the prism-like single crystal with Ag glue, and the device was placed in a shielding box during the measurement. Temperature-dependent electrical conductivities and *I–V* curves were measured on a single crystal sample with an appropriate size of 0.60 × 0.32 × 0.32 mm ($l \times w \times h$) by the two-probe method in a Keithley 2636B sourcemeter with a hot plate (MR Hei-Tec, Heidolph) as the heat source.

The conductivities (σ) were calculated through Eqs. (1) and (2). The active energy (E_a) was obtained by linear fitting of $1/kT$ *vs.* $\ln\sigma$ curve with Arrhenius formula, Eq. (3).

$$R = \frac{U}{I} \tag{1}$$

$$\sigma = \frac{l}{Rwh} \tag{2}$$

$$\ln(\sigma) = \ln(A) - \frac{E_a}{kT} \tag{3}$$

where σ is Conductivity; A is the pre-exponential factor; E_a is Activation energy; k is Boltzmann constant; T is the temperature (K). Note: unit conversion $1kT = 25$ meV, when $T = 300$ K.

3 Result and Discussion

Pale-yellow prism-like crystals of **1** are obtained by a solvent-thermal reaction of $Zn(NO_3)_2{\cdot}6H_2O$, TDC and TPT with the molar ratio of 5:3:2. Phase purity of the as-prepared crystalline materials is approved by powder X-ray diffraction (PXRD), infrared spectrum (IR) and elemental analysis (EA) (Figs. S1, S2). Single crystal X-ray diffraction analysis reveals that **1** is crystallized in the monoclinic $P2_1/c$ space group, which is an isostructural compound reported by our group and others [30, 31]. As shown in Fig. 1a, there are two independent Zn centers (Zn1 and Zn2) bridged by TPT and TDC molecules. The 5-coordinated Zn1 center lies in a pyramid geometry, coordinated with four oxygen atoms from four separated TDC molecules and one nitrogen atom from the pyridyl of TPT ligand. Adjacent zinc ions (Zn1) are connected by four carboxyl groups from four TDC ligands generating a paddle-wheel unit $[Zn_2(COO)_4]$. The Zn2 center is 6-coordinated with four oxygen atoms of two TDC molecules and two nitrogen atoms of two TPT molecules in a highly distorted triangular prism environment. The connections of TPT and TDC ligands with the Zn centers extend the structural motif to a 2D sheet along the *ab* plane (Fig. 1b). Another TDC ligand acting as a pillar further connects the 2D layer to a robust 3D framework with a topologic type of 3,4,6T32 (Fig. 1c). The void space of the 3D framework is filled with three independent equivalent frameworks giving rise to a triply-interpenetrated structure. This structural arrangement helps to shorten the distance between triazine moiety in TPT and the thienyl group in TDC. As shown in Fig. 1d, the molecules packing mode of the triazine group of TPT and the thiophene ring of TDC is a typical offset stacked configuration with a centroid–centroid interplanar distance of 4.083 Å. The nearest distance between the oxygen donor of TDC and the nitrogen atom of electron-deficient TPT is 3.627 Å, and the distance between the electron-rich sulfur atom and the nitrogen atom of TPT is 3.713 Å. All these D–A distance values satisfy the requirement for intermolecular electron transfer [32], indicating that

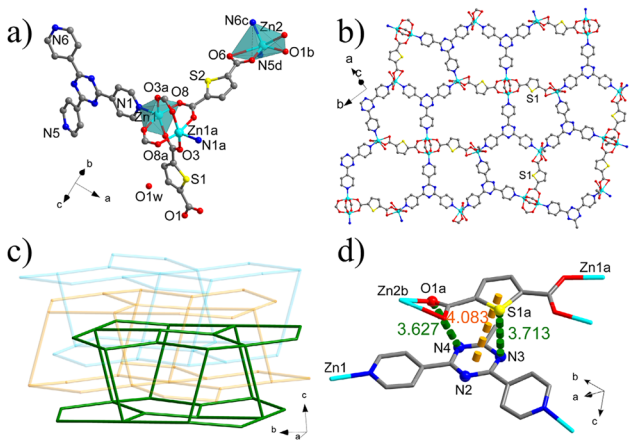

Fig. 1 View of **a** asymmetric units, **b** 2D network composed by TPT and S1-TDC, **c** tri-interpenetrating topological structure, and **d** π–π interaction between TPT and TDC in compound **1**

electrons can hop from either S or O donors to N acceptors upon external stimuli.

Solid state UV–vis spectrum of pale-yellow **1** displays two main absorption bands centered at ~ 320 and ~ 400 nm, corresponding to π–π* and n–π* transition of the aromatic rings (viz. triazine, pyridine and thiophene moieties) (Fig. 2). Upon light irradiation, the color of **1** changes from pale-yellow to green. A broad absorption peak ranging from ~ 520 to 800 nm centered at 600 nm emerges at the same time and gradually rises to the maximum in 4 min continuous irradiation. Green compound **1** can bleach reversibly by storing in the dark under ambient atmosphere after 5 cycles (Fig. 3). To illustrate the structural stability, the PXRD and IR spectra of **1** have been done after 5 cycles of reversible switching. As shown in Figures S1a and S2b, those spectra remain unchanged compared with the pristine one. It indicates that stimuli-response systems **1** do not show any structural or configurational changes, due to its rigid crystalline framework. Additionally, the generation of organic radicals is verified by the ESR measurement with a *g* value of 2.0087 (Fig. 4) [33].

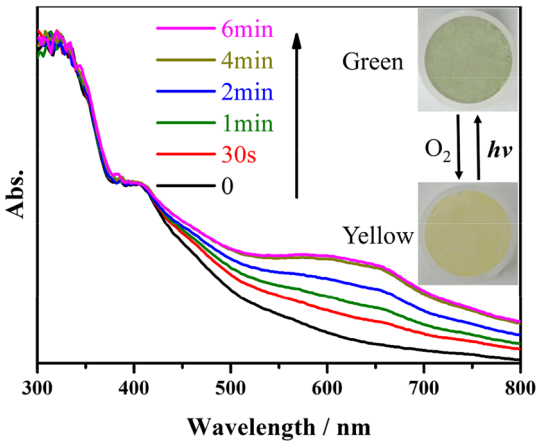

Fig. 2 UV–vis diffuse-reflectance spectral changes of **1** upon light irradiation (Xenon lamp CEL-TCX250, 290–800 nm)

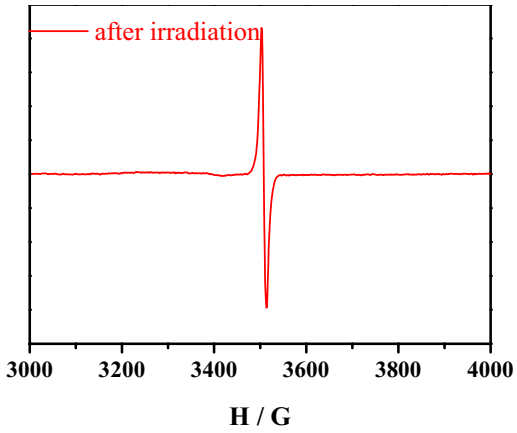

Fig. 4 ESR spectrum of **1** after light irradiation

XPS analysis reveals that electron-rich thienyl and carboxyl groups are electron donors and electron deficient triazine group of TPT is electron acceptor, approving well with the result of single crystal structure analysis. As shown in Figs. 5 and S4, XPS spectra of **1** before and after coloration are employed to verify the D–A mechanism of electron transfer. N 1s peak is deconvoluted into two peaks, which are referred to as pyridinic N and triazinic N respectively [34, 35]. After irradiation, the binding energy of pyridinic N remains unchanged (398.6 eV). In contrast, triazinic N yields a negative shift from 399.4 to 399.2 eV suggesting it is electron acceptor. To assess the role of S atoms of TDC during the photochromic changes, curve fitting of high-resolution S 2p peaks is performed. The S 2p spectrum of pale-yellow **1** shows only one peak at 163.6 eV, which can be resolved into two peaks with the binding energy located at 163.5 and 164.8 eV, corresponding to C–S–C 2p3/2 and C–S–C 2p1/2 respectively [36]. By comparison, a new peak emerges at 167.6 eV in the full spectrum of the green one after irradiation. This peak can be ascribed to high-valence-state sulfur, *e.g.* SO_x ($x = 1, 2, 3$), sulfonium ($C–S^+–C$) [37]. As no obvious change in the crystal phase and composition of **1** after irradiation, the new binding energy peak should

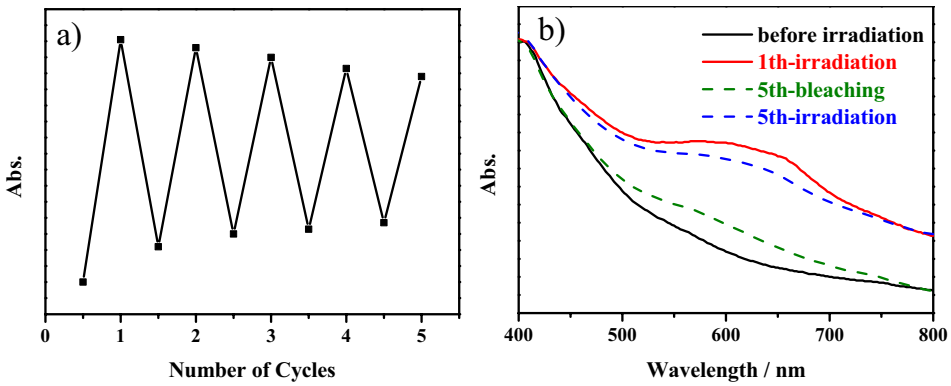

Fig. 3 UV–Vis absorbance **a** changes at 610 nm, and **b** selected spectral changes of compound **1** on alternate irradiation and bleached in the dark under ambient atmosphere over five cycles

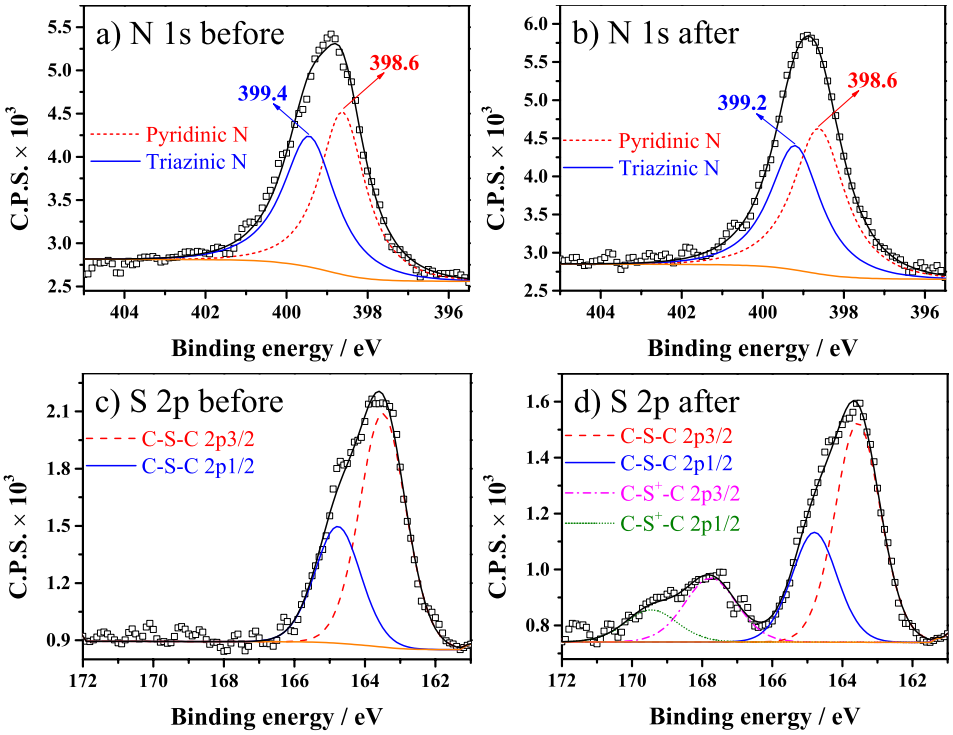

Fig. 5 N 1s peak and the peak fitting results of **1 a** before, and **b** after the color change; S 2p peak and the peak fitting results of **1 c** before, and **d** after the color change

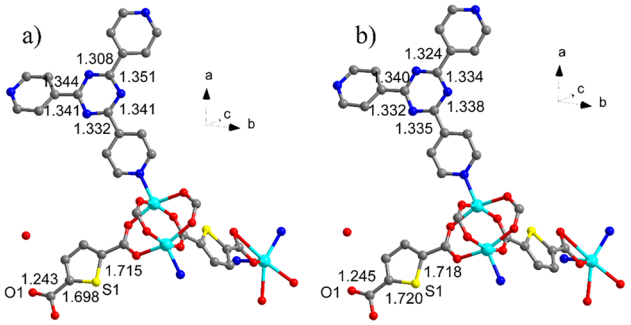

Fig. 6 View of asymmetric units of **1 a** before and **b** after light irradiation

be corresponding to sulfonium, which also can be deconvoluted into two peaks, viz. C–S^+–C 2p3/2 and C–S^+–C 2p1/2. These results confirm that the thienyl unit in TDC acts as the electron donor in the electron transfer reaction. For the binding energy of O 1s, the peak upshifts by ~ 0.4 eV after irradiation, indicating that electron dissociation occurred on O atoms of TDC during light-stimuli [38]. Thus, the carboxylate group also involves in electron transfer as donor.

Furthermore, the single-crystal XRD data after light irradiation was collected to intuitively confirm the mechanism of electron transfer. As shown in Fig. 6, and Tables S2 & S3, in comparison with the pristine one, the S1-C22 bond length in the crystal data of **1** after colorization is elongated by 0.022 Å, whereas the other bond distances, viz. C23-O1 and C-N in triazine, change slightly. It can be explained as follows. First, for the C23-O1 bond, the moiety of C23, O1 and O2 are disordered, which have been split into two parts. Therefore, no change in bond lengths is observed. Second, for the C-N bond in triazine, due to the conjugated effect, the C-N bond lengths in TPT tend to average out. Third, the obvious elongation in S1-C22 bond suggests that S atoms lose electrons which weakens the bond. Combining other characterizations (XPS, XRD and IR), it is concluded that photo-induced electrons hop from carboxylate groups / electron-rich thienyl-S in TDC to electron-deficient TPT.

The conductive behavior of **1** is investigated by single crystal conductivity measurements in a two-probe configuration. Pale-yellow **1** displays intrinsic conductivity of 4.3×10^{-9} S cm^{-1}, which decreases to 1.9×10^{-9} S cm^{-1} after light irradiation (Fig. 7), showing a photoconductive switching mode [4]. The calculated activation energy (E_a) also changes from 0.343 to 0.381 eV. As its value of conductivity is also coupled with the photochromic process, it gives out an interesting reversible photo-switchable conductance with color indication. This phenomenon can be interpreted by the structure and property relationships. Close packing structure of **1** with triply interpenetrated mode contributes to generating π–π interactions between D–A units, that trigger effective charge delocalization [4, 39, 40]. After irradiation, the photoexcited electron transfer from TDC to TPT decreases the electron density of the coordination chains, which substantially reduces the conductivity [4, 41]. The calculated charge-state density map of TDC based on single-crystal data indicates that the function values of S1 slightly decrease

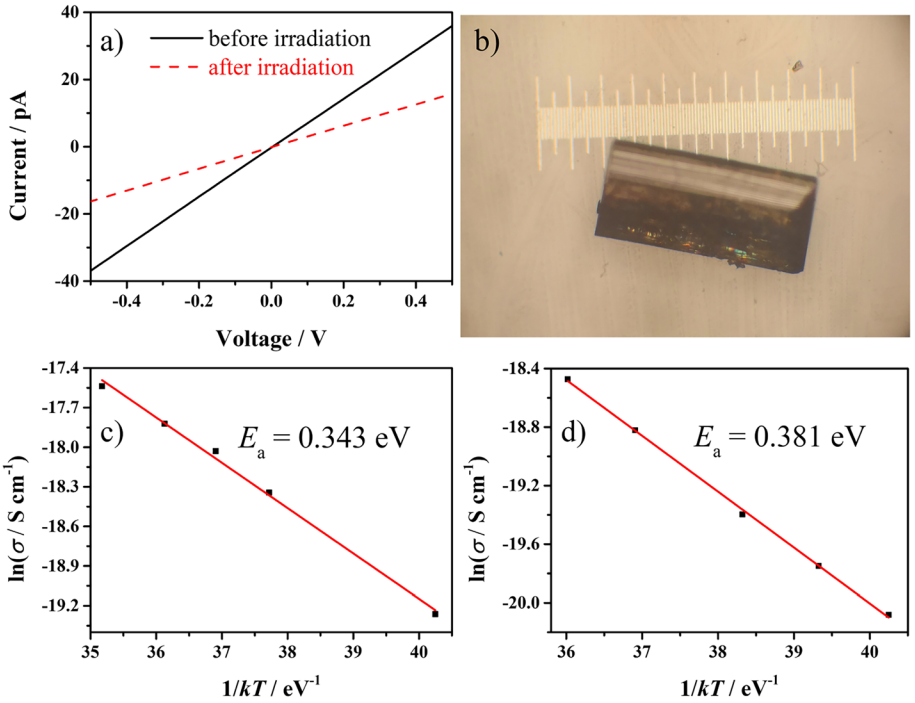

Fig. 7 **a** *I–V* characteristics of **1** before and after light irradiation, **b** photograph of the single crystal for conductivity measurements, Arrhenius plots **c** before and **d** after irradiation, where E_a is the activation energy

from 33.53 to 32.93 e Å^{-3} after light irradiation (Figure S6). It agrees with the XPS analysis result that the electron density of TDC decreases after the photo-coloration. XRD and thermogravimetric analysis (TGA) indicate that compound **1** remains in its crystalline form until 300 °C (Figs. S1b, S7). The good agreement of the peaks in the PXRD patterns before and after irradiation confirms that its framework structure keeps intact during the electron transfer reaction.

4 Conclusion

In summary, a single crystalline photoconducting switch with color indication is built based on the thienyl containing photosensitive zinc organic framework. Different from most reported single carboxyl group donors, a unique electron transfer phenomenon is observed in this study that both the thienyl group and carboxyl group involve in the electron transfer reaction as electron donors if their packing satisfies the requirement of D–A distance. The coupling with photochromic reaction decreases the electron density of TDC, creating a bifunctional photoactive device. It provides an effective way for designing visible photoconducting switches by the crystal engineering strategy.

5 Accession Codes

CCDC 2035073 and 2054909 contain the supplementary crystallographic data for this paper. These data can be obtained free of charge via www.ccdc.cam.ac.uk/data_request/cif, by emailing data_request@ccdc.cam.ac.uk, or by contacting The Cambridge Crystallographic Data Centre, 12, Union Road, Cambridge CB2 1EZ, UK; fax: + 44 1223 336033.

Supplementary Information The online version contains supplementary material available at https://doi.org/10.1007/s10904-023-02570-7.

Author Contributions AT, JZ and ZF contributed the central idea, performed research, analyzed data, and wrote the paper. JP and JL revised the manuscript. All authors reviewed the manuscript.

Funding The funding provided by the NSFC (21903026, 21975081), the Guangdong Basic and Applied Basic Research Foundation (2020A1515010378), the Research Fund Program of Guangdong Provincial Key Laboratory of Fuel Cell Technology (FC202212) and the SRP Program for financial support.

Declarations

Competing interests The authors declare no competing interests.

References

1. Y.J. Ma, J.X. Hu, S.D. Han et al., Manipulating on/off single-molecule magnet behavior in a Dy(III)-based photochromic complex. J. Am. Chem. Soc. **142**, 2682–2689 (2020)
2. O. Toma, N. Mercier, C. Botta, Process-dependent reversible mechanochromic luminescence of bismuth based polymorphs. J. Mater. Chem. C **4**, 5940–5944 (2016)
3. H. Houjou, T. Kato, H. Huang et al., Re-evaluation of the tert-butyl method in crystal engineering of salicylideneanilines by

simultaneous observation of photochromism and thermochromism in single crystals. Cryst. Growth Des. **19**, 1384–1390 (2019)
4. C. Sun, G. Xu, X.M. Jiang et al., Design strategy for improving optical and electrical properties and stability of lead-halide semiconductors. J. Am. Chem. Soc. **140**, 2805–2811 (2018)
5. C. Sun, M.S. Wang, G.C. Guo, Photochromic semiconductors with record-high dielectric permittivity gain at room temperature. ACS Appl. Electron. Mater. **3**, 3301–3305 (2021)
6. W. Liu, D. Banerjee, F. Lin et al., Strongly luminescent inorganic organic hybrid semiconductors with tunable white light emissions by doping. J. Mater. Chem. C **7**, 1484–1490 (2019)
7. T.L. Yu, Y.M. Guo, G.X. Wu et al., Recent progress of d^{10} iodoargentate(I)/iodocuprate(I) hybrids: structural diversity, directed synthesis, and photochromic/thermochromic properties. Coordin. Chem. Rev. **397**, 91–111 (2019)
8. O. Toma, M. Allain, F. Meinardi et al., Bismuth-based coordination polymers with efficient aggregation-induced phosphorescence and reversible mechanochromic luminescence. Angew. Chem. Int. Ed. **55**, 7998–8002 (2016)
9. N.N. Zhang, Y.F. Han, M.X. Du et al., 2,4,6-Tri(4-pyridyl)-1,3,5-triazine: photoinduced charge separation and photochromism in the crystalline state. Chemistry **25**, 13972–13976 (2019)
10. B.D. Ge, Y. Han, S.D. Han et al., Tunable photochromic properties of hybrid solids controlled by the conjugated length of non-photochromic units. Inorg. Chem. Front. **6**, 2435–2440 (2019)
11. T. Honda, T. Nakanishi, K. Ohkubo et al., Structure and photoinduced electron transfer dynamics of a series of hydrogen-bonded supramolecular complexes composed of electron donors and a saddle-distorted diprotonated porphyrin. J. Am. Chem. Soc. **132**, 10155–10163 (2010)
12. Y.J. Ma, J.X. Hu, S.D. Han et al., Photochromism and photomagnetism in crystalline hybrid materials actuated by nonphotochromic units. Chem. Commun. **55**, 5631–5634 (2019)
13. C. Sun, X.Q. Yu, M.S. Wang et al., A smart photochromic semiconductor: breaking the intrinsic positive relation between conductance and temperature. Angew. Chem. Int. Ed. **58**, 9475–9478 (2019)
14. N. Leblanc, W.H. Bi, N. Mercier et al., Photochromism, electrical properties, and structural investigations of a series of hydrated methylviologen halobismuthate hybrids: influence of the anionic oligomer size and iodide doping on the photoinduced properties and on the dehydration process. Inorg. Chem. **49**, 5824–5833 (2010)
15. L.Z. Cai, X.Y. Chen, M.S. Wang et al., Photochromic Lanthanide(III) materials with ion sensing based on pyridinium tetrazolate zwitterion. ACS Omega **4**, 7492–7497 (2019)
16. C.B. Aakeröy, N.R. Champness, C. Janiak, Recent advances in crystal engineering. CrystEngComm **12**, 22–43 (2010)
17. Z.J. Zhang, S.C. Xiang, G.C. Guo et al., Wavelength-dependent photochromic inorganic-organic hybrid based on a 3D iodoplumbate open-framework material. Angew. Chem. Int. Ed. **47**, 4149–4152 (2008)
18. J.Z. Liao, S.S. Wang, X.Y. Wu et al., Coordination-driven fast self-assembly of a charge-transfer hydrogel with reversible photochromism. Dalton Trans. **47**, 1027–1031 (2018)
19. Y.J. Ma, S.D. Han, J. Pan et al., An inorganic-organic hybrid framework from the assembly of an electron-rich diphosphonate and electron-deficient tripyridyl moiety. J. Mater. Chem. C **6**, 9341–9344 (2018)
20. H. Takezawa, T. Murase, G. Resnati et al., Halogen-bond-assisted guest inclusion in a synthetic cavity. Angew. Chem. Int. Ed. **54**, 8411–8414 (2015)
21. H. Pinfold, C. Greenland, G. Pattison et al., Fluorinated carboxylic acids as powerful building blocks for the formation of bimolecular monolayers. Chem. Commun. **56**, 125–128 (2020)
22. B.F. Abrahams, S.R. Batten, M.J. Grannas et al., Ni(tpt)$(NO_3)_2$-a three-dimensional network with the exceptional (12,3) topology: a self-entangled single net. Angew. Chem. Int. Ed. **38**, 1475–1477 (1999)
23. Y. Suenaga, H. Konaka, T. Sugimoto et al., Crystal structure and photo-induced property of two-dimensional silver (I) complex with 1, 3, 5-tris (benzylsulfanyl) benzene. Inorg. Chem. Commun. **6**, 389–393 (2003)
24. A. Aumüller, E. Hädicke, S. Hünig et al., Crystal structure and conductivity of a novel charge-transfer complex of N, N'-dicyano-1,4-naphthoquinonediimine and tetrathiafulvalene. Angew. Chem. Int. Ed. **23**, 449–450 (1984)
25. J. Ferraris, D.O. Cowan, V. Walatka et al., Electron transfer in a new highly conducting donor-acceptor complex. J. Am. Chem. Soc. **95**, 948–949 (1973)
26. U. Geiser, M.A. Beno, A.M. Kini et al., The crystal structures and physical properties of polymeric (BEDT-TTF)-metallothiocyanates. Synth. Met. **27**, A235–A241 (1988)
27. T. Kambe, R. Sakamoto, K. Hoshiko et al., π-Conjugated Nickel bis(dithiolene) complex nanosheet. J. Am. Chem. Soc. **135**, 2462–2465 (2013)
28. Y.L. Han, M. Hamada, I.Y. Chang et al., Fast T-type photochromism of colloidal Cu-doped ZnS nanocrystals. J. Am. Chem. Soc. **143**, 2239–2249 (2021)
29. H. Ito, D. Yoshioka, M. Hamada et al., Photochromism of colloidal ZnO nanocrystal powders under ambient conditions. Photochem. Photobiol. Sci. **21**, 1781–1791 (2022)
30. Z. Fu, Y. Chen, J. Zhang et al., Correlation between the photoactive character and the structures of two novel metal organic frameworks. J. Mater. Chem. **21**, 7895–7897 (2011)
31. X.R. Zhuang, X. Zhang, N.X. Zhang et al., Novel multifunctional Zn metal-organic framework fluorescent probe demonstrating unique sensitivity and selectivity for detection of PA and Fe^{3+} ions in water solution. Cryst. Growth Des. **19**, 5729–5736 (2019)
32. P.C. Jhang, N.T. Chuang, S.L. Wang, Layered zinc phosphates with photoluminescence and photochromism: chemistry in deep eutectic solvents. Angew. Chem. Int. Ed. **49**, 4200–4204 (2010)
33. Q.Z. Li, W.L. Hou, F. Peng et al., Photothermal conversion performance of perylene diimide radical anion salts modified with tunable moieties. J. Mater. Sci. **54**, 217–227 (2019)
34. C. Malitesta, M.R. Guascito, E. Mazzotta et al., X-ray photoelectron spectroscopy characterization of electrosynthesized poly (3-thiophene acetic acid) and its application in Molecularly Imprinted Polymers for atrazine. Thin Solid Films **518**, 3705–3709 (2010)
35. D.Y. Osadchii, A.I. Olivos-Suarez, A.V. Bavykina et al., Revisiting nitrogen species in covalent triazine frameworks. Langmuir **33**, 14278–14285 (2017)
36. A.D. Tan, K. Wan, Y.F. Wang et al., N, S-containing MOF-derived dual-doped mesoporous carbon as a highly effective oxygen reduction reaction electrocatalyst. Catal. Sci. Technol. **8**, 335–343 (2018)
37. B. Lindberg, K. Hamrin, G. Johansson et al., Molecular spectroscopy by means of ESCA II. Sulfur compounds. Correlation of electron binding energy with structure. Phys. Scripta **1**, 286 (1970)
38. B. Folkesson, P. Sundberg, L. Johansson et al., An ESCA investigation of some copper complexes. J. Electron Spectrosc. Relat. Phenom. **32**, 245–256 (1983)
39. J. Zhang, G. Zhao, Y. Qin et al., Enhancement of the p-channel performance of sulfur-bridged annulene through a donor-acceptor co-crystal approach. J. Mater. Chem. C **2**, 8886–8891 (2014)
40. Z. Guo, D.K. Panda, K. Maity et al., Modulating the electrical conductivity of metal–organic framework films with intercalated guest π-systems. J. Mater. Chem. C **4**, 894–899 (2016)

41. J.Z. Liao, J.F. Chang, L. Meng et al., Lone pair-π interaction-induced generation of photochromic coordination networks with photoswitchable conductance. Chem. Commun. **53**, 9701–9704 (2017)

Authors and Affiliations

Aidong Tan[1,2] · Jie Zhang[1] · Jinhua Piao[3] · Jiayao Li[1] · Zhiyong Fu[1]

✉ Jie Zhang
cejzhang@scut.edu.cn

✉ Zhiyong Fu
zyfu@scut.edu.cn

[1] Key Laboratory on Fuel Cell Technology of Guangdong Province, School of Chemistry and Chemical Engineering, South China University of Technology, Guangzhou 510641, People's Republic of China

[2] Institute of Energy Power Innovation, North China Electric Power University, Beijing 102206, People's Republic of China

[3] School of Food Science and Engineering, South China University of Technology, Guangzhou 510641, People's Republic of China